Development/Plasticity/Repair

Mediolateral Compartmentalization of the Cerebellum Is Determined on the "Birth Date" of Purkinje Cells

Mitsuhiro Hashimoto[1] **and Katsuhiko Mikoshiba**[1,2]

[1]Laboratory for Developmental Neurobiology, RIKEN BSI, 2-1 Hirosawa, Wako-shi, Saitama 351-0198, Japan, and [2]Department of Molecular Neurobiology, The Institute of Medical Science, The University of Tokyo, Tokyo 108-8639, Japan

The adult cerebellum is functionally compartmentalized into clusters along the mediolateral axis (M-L clusters), and a variety of molecular makers are expressed in specific subsets of M-L clusters. These M-L clusters appear to be the basic structure in which cerebellar functions are performed, but the mechanisms by which cerebellar mediolateral compartmentalization is established are still unclear. To address these questions, we examined the development of M-L clusters using replication-defective adenoviral vectors. The adenoviral vectors effectively introduced foreign genes into the neuronal progenitor cells of the cerebellum in a birth date-specific manner, allowing us to observe the native behavior of each cohort of birth date-related progenitor cells. When the adenoviral vectors were injected into the midbrain ventricle of mouse embryos on embryonic days 10.5 (E10.5), E11.5, and E12.5, the virally infected cerebellar progenitor cells developed into Purkinje cells. Notably, the Purkinje cells that shared the same birth date formed specific subsets of M-L clusters in the cerebellum. Each subset of M-L clusters displayed nested and, in part, mutually complementary patterns, and these patterns were unchanged from the late embryonic stage to adulthood, suggesting that Purkinje cell progenitors are fated to form specific subsets of M-L clusters after their birth between E10.5 and E12.5. This study represents the first such direct observation of Purkinje cell development. Moreover, we also show that there is a correlation between the M-L clusters established by the birth date-related Purkinje cells and the domains of *engrailed-2*, *Wnt-7B*, *L7/pcp2*, and EphA4 receptor tyrosine kinase expression.

Key words: **compartmentalization; cerebellum; neuronal birth date; Purkinje cell; adenoviral vector; development**

Introduction

Earlier anatomical and physiological studies have revealed that the cerebellar cortex is compartmentalized into a series of bilaterally symmetric clusters along the mediolateral (M-L) axis (for review, see Oscarsson, 1980; Voogd and Bigare, 1980; Ito, 1984; Voogd and Glickstein, 1998). For instance, terminals of climbing fibers that originate from specific subnuclei of the inferior olive innervate the contralateral cerebellar cortex and organize into mediolateral stripes (M-L clusters). Furthermore, the Purkinje cells (PCs) within each M-L cluster of climbing fibers project to a particular region in the cerebellar deep and vestibular nuclei. Electrophysiological experiments have indicated that the M-L clusters of the climbing fibers provide a somatotopic map that encodes the spatial components of a movement (Robertson and Laxer, 1981; Bloedel and Kelly, 1991; Garwicz, 2000), implying that the cerebellar M-L clusters are basic units of cerebellar function.

Recent molecular biological analyses have also revealed that a variety of molecular markers are expressed in specific M-L clusters (for review, see Hawkes and Gravel, 1991; Hawkes, 1997; Herrup and Kuemerle, 1997; Oberdick et al., 1998). For example, *L7/pcp-2* expression is restricted to PCs that form M-L clusters after E15.5 (Oberdick et al., 1993). Homologs of the *Drosophila* segment polarity genes *engrailed* (*En*)*-1*, *En-2*, *Pax-2,* and *Wnt-7B* are also expressed in specific subsets of M-L clusters between E15.5 and E17.5, and the expression patterns of *En-2* and *Wnt-7B* complement one other; that is, they are present in mutually exclusive regions and may compensate for each other's function (Millen et al., 1995). The adult cerebellum is also compartmentalized into specific subsets of M-L clusters, as demonstrated by the expression patterns in PCs of other M-L markers such as zebrin I and II (Leclerc et al., 1988). The M-L cluster patterns of zebrin I and II correlate closely with the projection pattern of climbing and mossy fibers (Gravel et al., 1987; Gravel and Hawkes, 1990; Wassef et al., 1991; Paradies et al., 1996) and with physiological activity (Chockkan and Hawkes, 1994; Chen et al., 1996; Hallem et al., 1999). These findings suggest that the compartmentalization of the cerebellum is regulated by specific molecular mechanisms and that the neural circuitry and morphology of the cerebellum are established on the basis of these M-L clusters.

However, the most basic questions regarding cerebellar M-L compartmentalization are not yet solved: what determines the pattern of M-L clusters, and when does it occur? The expression of M-L makers is often transient or variable (for review, see Herrup and Kuemerle, 1997; Oberdick et al., 1998). This obstacle

Received May 21, 2003; revised Oct. 21, 2003; accepted Oct. 22, 2003.

This work was supported by Special Coordination Funds of the Ministry of Education, Culture, Sports, Science, and Technology of the Japanese Government. We thank Drs. T. Furuich, T. Miyata, M. Ogawa, and M. Yuzaki, and especially Dr. R. Hawkes for helpful discussion and comments on this manuscript, and Drs. N. Morita, A. Sato, and T. Furuich for providing a great technique of whole-mount *in situ* hybridization and antisense RNA probes specific to *En-2*, *Wnt-7B,* and *L7/pcp2* genes.

Correspondence should be addressed to Dr. Mitsuhiro Hashimoto, Laboratory for Developmental Neurobiology, RIKEN BSI, 2-1 Hirosawa, Wako-shi, Saitama 351-0198, Japan. E-mail: mhashimoto@brain.riken.go.jp.

 0270-6474/03/2311342-10$15.00/0

makes it difficult to determine the process by which the M-L clusters are established and to clarify the interrelationships between M-L clusters.

To address these questions, we attempted to label each subset of PCs that share the same birth date using replication-defective adenoviral vectors, and to examine the native behavior of each subset. Our results indicate that the PC progenitor cells are already destined to form specific subsets of M-L clusters on their neuronal birth dates.

Materials and Methods

Preparation of recombinant adenoviral vectors. The adenoviral vector is based on human adenovirus type 5 (Ad5), rendered replication-incompetent by deletion of the E1A, E1B, and E3 regions of their genome. The adenoviral vector AdexCAG-NL-LacZ (Hashimoto et al., 1996) expresses nuclear-targeted β-galactosidase (NL-LacZ) under the control of a strong, ubiquitous CAG promoter based on the chicken β-actin promoter (Niwa et al., 1991). AdexCAG-HSVtk expresses Herpes simplex virus thymidine kinase (HSVtk) as a suicide gene under the control of the CAG promoter. AdexCAG-HSVtk was constructed as follows. A 2.8 kbp *Bgl*II–*Bam*HI fragment from pTKS (Wigler et al., 1978) coding HSVtk and polyadenylation signal was inserted into the *Swa*I cloning site of pAdex1pCAw (Hashimoto et al., 1996), and then the pAdexCAG-HSVtk cosmid vector was constructed. The adenoviral vector, AdexCAG-HSVtk, was derived from pAdexCAG-HSVtk using a modification of COS–TPC method (Miyake et al., 1996). The adenoviral vectors are based on human adenovirus type 5 (Ad5), and is replication-incompetent because it lacks the E1A, E1B and E3 regions of its genome. Each clone was checked by restriction enzymatic digestion (restriction analysis) and PCR for E1A (Zhao et al., 1998) to not include parent adenoviruses (Ad5). Adenoviral vectors were purified and concentrated by double cesium step gradient centrifugation (Hashimoto et al., 1996). The titers of viral stocks were determined by plaque assay on human embryonic kidney 293 cells.

Injection of adenoviral vector. Pregnant ICR mice (Slc:ICR; Nippon-SLC, Japan) were housed in a controlled environment (RIKEN BSI animal facility) under a regulated 12 hr light/dark cycle. All procedures involving animal preparation were approved by the RIKEN BSI Animal Committee. The day on which a vaginal plug was detected was counted as embryonic day 0.5 (E0.5).

Manipulation of mouse embryos was performed according to a modification of *exo utero* surgery (Muneoka et al., 1986; Turner and Cepko, 1987). Adenoviral vectors (total 1×10^8 pfu) were injected into the midbrain ventricle of embryos on E10.5, E11.5, E12.5, and E13.5. To ablate the M-L clusters, AdexCAG-HSVtk or a 1:1 mixture of AdexCAG-HSVtk and AdexCAG-NL-LacZ was injected into the embryos on E12.5. Twenty-four hours after the injection, the pregnant dams were injected intraperitoneally with 30 mg/kg body weight ganciclovir (GCV; Sigma-Aldrich, Tokyo, Japan). The manipulated embryos were collected at various developmental stages. The surviving embryos at E18.5 were delivered by Cesarean section, and they were fostered to dams. The next day, E19.5, was designated as postnatal day 0 (P0). Four pregnant mice, each with 8–10 embryos on the manipulated side of the uterine horn, were injected with the adenoviral vectors and analyzed for each experiment. The manipulated animals were maintained in a clean environment.

BrdU labeling. A mixture of AdexCAG-NL-LacZ (total 2.5×10^7 pfu) and bromodeoxyuridine (BrdU; Sigma-Aldrich; total 2.5 μg) was injected into the midbrain ventricle of mouse embryos on E11.5 or E12.5. At E18.5, the embryos were fixed and sectioned transversely as described below.

Histochemical analysis. Mice injected with the adenoviral vector were fixed with 4% paraformaldehyde (PFA) in a 0.1 M phosphate buffer (PB), pH 7.4. To detect β-galactosidase (β-gal) activity, fixed whole brains and embryos were stained with Bluo-gal (Invitrogen, Tokyo, Japan) solution (Hashimoto et al., 1996). Tissue was cryoprotected by serial equilibration in sucrose [10, 15 and 20% (w/v) in PBS(−)] at 4°C. In some cases, brains were sliced transversely, aided by Brain Matrices (15003; Ted Pella, Inc., Redding, CA). Tissues and embryos were frozen in a Tissue-Tek O.C.T. compound (Sakura Finetech U.S.A., Inc.). They were sectioned on a cryostat (JUNG CM3000, Germany), rinsed in PBS(−), and either used for immunohistochemistry or counterstained with neutral red (Sigma-Aldrich).

Immunohistochemistry. Cryostat sections were treated as described (Hashimoto et al., 1996) with polyclonal antibodies against calbindin D_{28K} (1:500; Chemicon International, Hofheim, Germany), EphA4, ephrin-A2, and ephrin-B2 (1:25; R & D Systems Inc., Minneapolis, MN). Immunoreactivity against each protein was detected using an ABC kit (Vector Laboratories, Burlingame, CA) and 3, 3′-diaminobenzidine tetrahydrochloride (DAB; DojnDo, Tokyo, Japan). Some sections were counterstained with cresyl violet (Merck Ltd., Tokyo, Japan). Cryostat sections of the BrdU-labeled brains were double-immunostained with monoclonal anti-BrdU (1:100; BD Biosciences) and rabbit polyclonal anti-β-gal (1:50; ICN/Cappel, Aurora, OH). BrdU and β-gal immunoreactivity was detected with rhodamine-conjugated goat anti-mouse IgG (ICN Biochemicals) and FITC-conjugated goat anti-rabbit IgG (ICN Biochemicals), respectively.

Whole-mount in situ *hybridization.* Whole-mount *in situ* hybridization was performed according to a modification of a previous report (Osumi-Yamashita et al., 1997). The antisense RNA probes for mouse *En-2*, *Wnt-7B,* and *L7/pcp2* genes were synthesized from the template plasmids. The cDNAs were amplified by PCR with the following primers: *En-2*, 5′-CCACAATGTCTTCTGTTTAGTG-3′ and 5′-GTCACAATTTTGATAACCACAG-3′; *Wnt-7B*, 5′-ATCTTTTACGTGTTTCTCTGCT-3′ and 5′-CTGGTTGTAGTAGCCTTGCT-3′; *L7/pcp2*, 5′-GTACTAGGATTTAGGGGCACTT-3′ and 5′-CTAGAACTCTCAAGGAGCTTGT-3′.

Results

Throughout this report, we use abbreviations in the form of "E11.5:P20." The left side indicates the embryonic stage at which the adenoviral vector was injected, and the right side ("P20") is the age at which the mice were analyzed.

M-L clusters in adult cerebella

AdexCAG-NL-LacZ, an adenoviral vector expressing nuclear-targeted β-gal, was injected into the midbrain ventricle of mouse embryos on E11.5, E12.5, and E13.5. Twenty days after birth (P20), each manipulated brain was Bluo-gal-stained by whole-mount for β-gal. High β-gal activity was observed in PCs in the E11.5:P20 (Fig. 1*A,B*) and E12.5:P20 (Fig. 1*C,D*) cerebella. In contrast, there was little β-gal activity in the E13.5:P20 (Fig. 1*E*), E14.5:P20 and E15.5:P20 (data not shown) cerebella. Interestingly, β-gal-positive PCs in the E11.5:P20 and E12.5:P20 cerebella formed an M-L array of clusters. The M-L clusters continued without interruption from the posterior into the anterior lobe. The pattern of β-gal-positive M-L clusters in the E11.5:P20 cerebellum was completely different from that in the E12.5:P20 cerebellum. In the E11.5:P20 cerebellum, five M-L clusters without β-gal-positive PCs were observed (Fig. 1*A,B,* arrowheads) in the midline vermis, the junction between the vermis and the hemisphere (paravermian region), and midway across each hemisphere. Label was also detected in the anterior half of the paraflocculus (PF) of the E11.5:P20 cerebellum. In contrast, in the E12.5:P20 cerebellum, β-gal-positive PCs were restricted to three M-L clusters (Fig. 1*C,D*): one in the midline vermis, and the others in a symmetrical pattern at the medial edge of each hemisphere. The PF of the E12.5:P20 cerebellum was negative for β-gal (Fig. 1*C,D*). To compare the M-L clusters in E11.5:P20 (Fig. 1*B*) and E12.5:P20 cerebella (Fig. 1*D*), we overlaid these images using Adobe Photoshop 6.0 (Fig. 1*F*). The β-gal-positive E12.5:P20 cluster at the cerebellar midline (colored yellow) colocalized with the β-gal-negative E11.5:P20 cluster, and the β-gal-positive E12.5:P20 clusters in the hemispheres overlapped with the E11.5:P20 clusters.

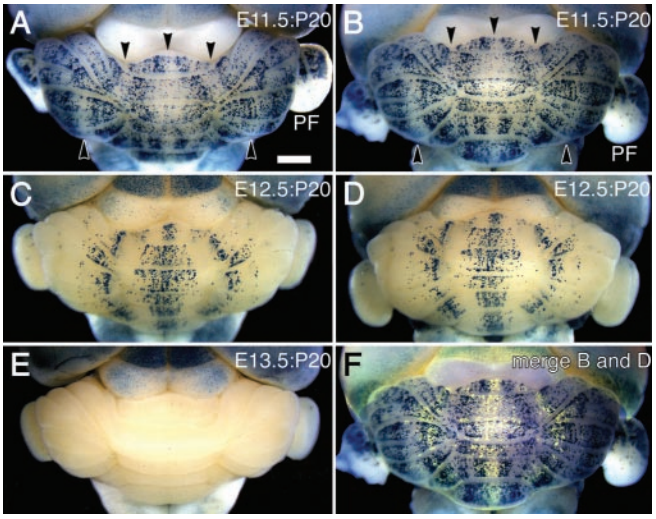

Figure 1. Comparison of M-L clusters in the adult cerebellum. AdexCAG-NL-LacZ was injected into the midbrain ventricles of embryos at E11.5, E12.5, and E13.5. At P20, each manipulated brain was stained by whole-mount for β-gal. Dorsal views of the E11.5:P20 (*A*), E12.5:P20 (*C*), and E13.5:P20 (*E*) cerebella are indicated. Posterior views of the E11.5:P20 (*A*) and E12.5:P20 (*C*) cerebella are shown in *B* and *D*, respectively. β-gal-positive PCs (blue) formed M-L clusters. The arrowheads in *A* and *B* indicate β-gal-negative clusters. *F* is a merge of *B* and *D*, in which blue is converted to yellow. PF, Paraflocculus. Scale bar, 1 mm.

Because the CAG promoter is ubiquitous in the rodent cerebellum, its transcriptional activity is not regulated by any intrinsic regulatory factors for gene expression. In fact, the cerebella of Z/AP transgenic mice (Lobe et al., 1999), which express the LacZ gene under the control of the CAG promoter, were uniformly stained with Bluo-gal (data not shown). In addition, when AdexCAG-NL-LacZ was injected directly into an adult cerebellum, there was no cell-type specificity of β-gal expression (Hashimoto et al., 1996). Consequently, the M-L clusters in this report are not simply artifacts caused by region-specific transcriptional activity of the CAG promoter.

These results indicate that it is possible to introduce certain genes into the PC progenitor cells using this technique. In addition, the PCs infected with AdexCAG-NL-LacZ appear to be localized to specific M-L clusters within the adult cerebellum, and the pattern of the M-L clusters labeled depends on the day of adenoviral injection.

BrdU labeling on E11.5 and E12.5

To determine the birth date of virally infected PCs, we directly injected BrdU together with AdexCAG-NL-LacZ into the midbrain ventricles of embryos on E11.5 and E12.5. The progenitor cells of PCs that undergo terminal DNA replication at the time of injection are strongly labeled with BrdU, because they do not divide any further. After injection of the BrdU/AdexCAG-NL-LacZ mixture, we transversely sectioned the E11.5:E18.5 and E12.5:E18.5 cerebella on a cryostat. The sections of E12.5:E18.5 cerebellum were stained for β-gal (Fig. 2*A*), and the other sections were immunostained with an anti-BrdU antibody (Fig. 2*B*). The distribution of β-gal-positive PCs (Fig. 2*A,* blue stains) coincided with the distribution of BrdU-labeled cells (Fig. 2*B*, black dots). This suggests that the virally infected PCs undergo terminal mitosis on E12.5. The transverse sections of the E11.5:E18.5 cerebellum were double-immunostained with anti-β-gal (Fig. 2*C*) and anti-BrdU (Fig. 2*D*) antibodies. The β-gal and BrdU immunoreactivities were colocalized in the PCs of the Purkinje cell layer (PL) and the neurons of the dentate nucleus (DN), one of the deep cerebellar nuclei (Fig. 2*E*). PCs and the deep cerebellar nuclear neurons arise from common progenitor cells from the ventricular zone of the fourth ventricle (Mathis et al., 1997). The germinal trigon (GT) and external granular layer (EGL: future molecular layer) were negative for anti-β-gal and anti-BrdU antibodies (Fig. 2*E*). GT and EGL may not be infected with adenoviral vectors because they are generated after termination of PC neurogenesis (Altman and Bayer, 1978). Consequently, these results indicate that BrdU-labeling and adenoviral infection occur simultaneously in single PC progenitor cells. The birth date of the virally infected PCs corresponds with the day of adenoviral injection, using this adenovirus-mediated gene transfer protocol.

Together with the above results, these observations indicate the following: adenoviral vectors can introduce foreign genes into a subset of cerebellar progenitor cells in a neuronal birth date-specific manner; the birth date-related PCs form a specific subset of M-L clusters; and the pattern of M-L clusters is determined by the PC birth date. How are these individual M-L clusters generated? To address this question, we analyzed M-L cluster development from embryonic stages to adulthood.

Development of M-L clusters

AdexCAG-NL-LacZ was injected into embryos on E11.5 and E12.5, and, subsequently, they were fixed and stained by whole-mount for β-gal at different ages (Fig. 3). To explain the relative positions of M-L clusters in the cerebellum at each developmental stage, we normalize the cerebellar widths and organize them as in Figure 3.

In E11.5:E12.5 brain (Fig. 3*A*), β-gal activity is already observed in the ventricular zones of the cerebellar primordium (CP), precerebellar neuroepithelium (PCN), and other ventricular zones of the fourth ventricle. In transverse sections of the E11.5:E12.5 cerebellum, β-gal-positive cells (presumptive PCs) occupied the ventricular zone of the CP (see Fig. 8*A*, arrow), and another cell group (presumptive deep cerebellar nuclear neurons) existed in the dorsal part of the CP (see Fig. 8*A*, arrowhead). Those β-gal-positive cells were not arranged in cluster-like formations within the ventricular zone of the CP. In E11.5:E14.5 cerebella (Figs. 3*B*, 8*B*), two symmetrical β-gal-positive clusters are seen within each CP (Figs. 3*B*, 8*B,* arrows, arrowheads). The clusters indicated by the arrows are horizontal in shape. They may be transformed into an M-L cluster because the CP rapidly expands to the cerebellar midline (see Fig. 8*B–D*). In E11.5:E16.5 cerebella (Fig. 3*C*), several clusters were observed, with β-gal activity weaker in the medial clusters than in the lateral clusters. In E11.5:E18.5 cerebella (Fig. 3*D*), the M-L clusters became clearer, indicating M-L compartmentalization of the cerebellum. Comparison of the E11.5:E16.5 and E11.5:E18.5 cerebella suggests that the M-L clusters generated on E11.5 are formed progressively in a lateral-to-medial sequence. The pattern of M-L clusters within the E11.5:E18.5 cerebellum was symmetrical around the midline; thus, the M-L clusters were numbered from 1 to 8 (see Fig. 5), with one midline cluster (1) and seven bilaterally symmetrical clusters (2–8) on either side of it. In E11.5:E18.5 cerebella (Figs. 3*D,* 5), clusters 1, 3, and 6/7 were completely negative for β-gal, and clusters 2, 4/5, and 8 were positive. The relative positions of clusters 2, 4/5, and 8 are indicated by white dotted lines in the left column. From E18.5 to E20, clusters 2, 4/5, and 8 were positive for β-gal, whereas clusters 1, 3, and 6/7 were always β-gal-negative (Fig. 3*D–I*). The relative positions of M-L clusters did not change, although their absolute locations were modified somewhat as the cerebellum underwent foliation. The E11.5:P20 cerebellum (Fig. 3*H*) was sliced transversely in the

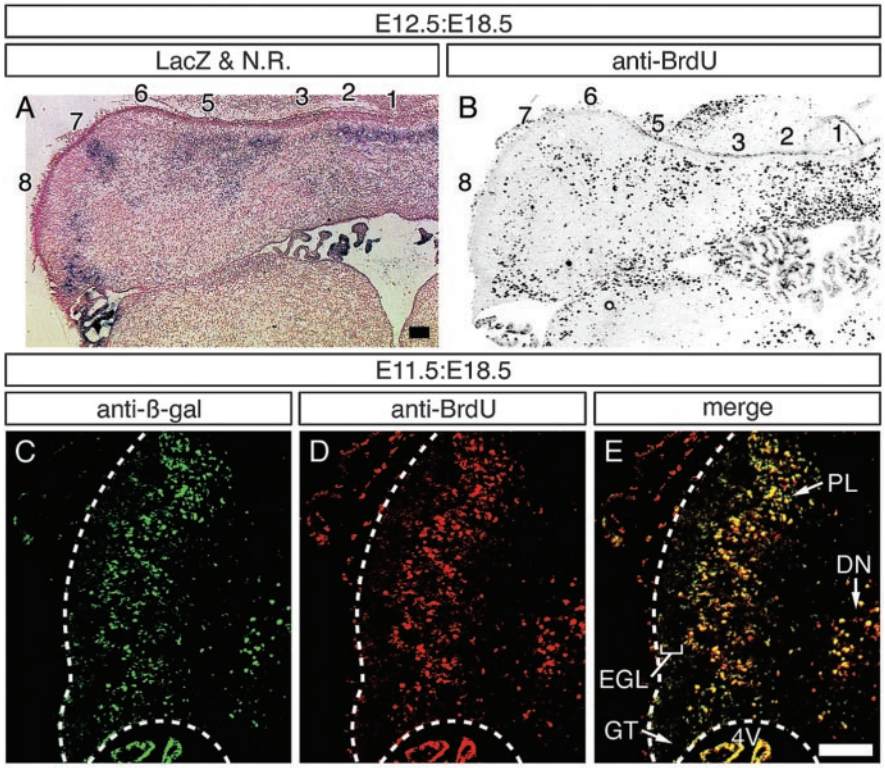

Figure 2. BrdU labeling of the cerebellum on E11.5 or E12.5. BrdU was injected into the midbrain ventricles of embryos at E11.5 and E12.5, together with AdexCAG-NL-LacZ. Transverse cryosections from the E12.5:E18.5 cerebellum were stained for β-gal (dark blue) and with neutral red (*A*, LacZ & N.R.). The other sections were stained with anti-BrdU (black) (*B*, anti-BrdU). Transverse sections from the E11.5:E18.5 cerebellum were double-immunostained with anti-β-gal (*C*, green) and anti-BrdU (*D*, red). *E* indicates the merged view of *C* and *D*. Numbers 1–8, The number of M-L clusters (refer to Fig. 5); 4V, fourth ventricle; DN, dentate nucleus; EGL, external granular layer; GT, germinal trigone; PL, Purkinje cell layer. Scale bars: *A* (for *A*, *B*), *E* (for *C*–*E*), 100 μm.

region indicated between the arrowheads (Fig. 3*I*). β-gal-positive cells were localized in the PL and deep nuclei, not in the granular layer (GL) or the white matter (wm). All β-gal-positive cells in the cerebellar cortex were PCs.

M-L clusters were also observed in the E12.5:16.5 cerebellum (Fig. 3*J*), but the pattern of M-L clusters was different from that of the E11.5:E16.5 cerebellum (Fig. 3*C*). In E12.5:E16.5 cerebella (Fig. 3*J*), the β-gal activity in the medial clusters was stronger than in the lateral clusters. The medial clusters (1 and 2) were first revealed in the E12.5:E16.5 cerebellum (Fig. 3*J*: compare with E11.5:E16.5 in Fig. 3*C*). In E12.5:E18.5 cerebella (Fig. 3*K*), the M-L clusters became clearer. Clusters 3/4, 6, and 8 were completely negative for β-gal, and clusters 1, 2, 5, and 7 were positive for β-gal. The positions of clusters 1, 5, and 7 are marked by white dotted lines in the right column. From E18.5 to P61, clusters 1, 2, and 5 remained positive for β-gal, whereas the others were β-gal-negative (Fig. 3*J*–*Q*). The pattern of M-L clusters did not change from E18.5 to P61, except for cluster 7, in which β-gal activity faded away by P10 (Fig. 3*N*). An E12.5:P20 cerebellum (Fig. 3*O*) was sectioned transversely in the region between the arrowheads, as shown in Figure 3*P*. The β-gal-positive cells in the cerebellar cortex are PCs.

These results indicate that each basic pattern of birth date-specific M-L clusters is established by E18.5, after which it does not change from the late embryonic stages through adulthood, even though the expression of all available M-L markers is transient and variable (for review, see Herrup and Kuemerle, 1997; Oberdick et al., 1998).

Immunohistochemistry of the E12.5:E18.5 cerebellum

Eph receptors and ephrin ligands are guidance molecules involved with regionalization and axon guidance in the developing brain (for review, see Wilkinson, 2001), and a recent study demonstrated that they are expressed within restricted M-L clusters in the developing chick cerebellum (Karam et al., 2000). Thus, we hypothesized that these molecules are involved with the specific pattern formation of M-L clusters. To examine this hypothesis, we stained horizontal and transverse sections of E12.5:E18.5 cerebella for β-gal and further immunostained them with anti-EphA4, anti-ephrin-A2, or anti-ephrin-B2 antibodies. EphA4 immunoreactivity was clearly restricted to M-L striped clusters within the E12.5:E18.5 cerebellum (Fig. 4*D*–*F*, column *B*), but ephrin-A2 and ephrin-B2 were undetectable. Interestingly, the EphA4-immunoreactive regions corresponded with clusters 2, 5, 7, and 8 (Fig. 4, column *B*); in clusters 2, 5, and 7, β-gal-positive PCs were found exclusively within the EphA4-positive regions (Fig. 4*D*–*F*, column *B*, arrows). Although β-gal positive PCs were absent from clusters 3/4 and 6 in the E12.5:E18.5 cerebellum (Fig. 4, columns *A*,*B*), calbindin D_{28K} (CaBP)-positive PCs were present in clusters 3/4 and 6 (Fig. 4, column *C*). The β-gal-positive PCs in E12.5:E18.5 cerebellum seem not to localize to the neighboring clusters 3/4 and 6, which are all EphA4-negative regions (Fig. 4*D*–*F*).

Cluster 8 in the E12.5-E18.5 cerebellum shows a fiber-like formation that is EphA4-positive but CaBP-negative (Fig. 4, asterisks). In the embryonic brain, the inferior cerebellar peduncle, a bundle of climbing fibers, is positive for EphA4 (data not shown). Moreover, the EphA4 expression pattern, in particular its expression in cluster 7 of the E12.5:E18.5 cerebellum (Fig. 4*E*), is similar to the projection pattern of climbing fibers, as previously described (Paradies et al., 1996). Accordingly, the climbing fibers seem to express EphA4. These results suggest that M-L cluster formation correlates with the EphA4 expression pattern in climbing fibers.

M-L patterns in late embryogenesis

PCs born on E11.5 and E12.5 did not contribute to the formation of clusters 3 and 6 (Fig. 3). It is also clear that PCs born on E10.5 comprise clusters 3 and 6 (Fig. 5, top line) and the posterior half of the adult PF (data not shown). Consequently, all cerebellar M-L clusters are produced during only three embryonic days from E10.5 to E12.5, and the birth date of PCs determines the time at which each M-L cluster is generated from the ventricular zone of the fourth ventricle.

To clarify the correlation between PC birth dates and cerebellar M-L cluster patterning at late embryonic stages, we compared the M-L clusters of E10.5:E18.5, E11.5:E18.5, and E12.5:E18.5 cerebella (Fig. 5). These M-L clusters were also compared with the EphA4-positive regions in horizontal and transverse sections

of the E12.5:E18.5 cerebellum (Fig. 4, data not shown). The E10.5:E18.5 cerebellum ("E10.5:E18.5" line in Fig. 5) shows clusters 3, 6, and 8, but cluster 8 is ambiguous because it is positive for β-gal in the near lateral view, but not in the dorsal view. In the E11.5:E18.5 cerebellum ("E11.5:E18.5" line in Fig. 5), clusters 2, 4, 5, and 8 are clearly demarcated, and in the E12.5:E18.5 cerebellum ("E12.5:E18.5" line in Fig. 5), clusters 1, 2, 5, and 7 can be seen clearly. Clusters 3 and 6 in the E10.5:E18.5 cerebellum compensate for gaps of M-L clusters in the E11.5:E18.5 and E12.5-E18.5 cerebella. Their positional correlation is shown in the diagram at the bottom of Figure 5. These M-L clusters can be classified into two categories. The first category consists of independent clusters that are generated on a particular day: clusters 1 (E12.5), 3 (E10.5), 4 (E11.5), 6 (E10.5), and 7 (E12.5). These clusters are all negative for EphA4, except for cluster 7, which is restricted to a very narrow region (Fig. 4*E* and lateral views in Fig. 5). The second category consists of clusters that are generated over 2 d and coincide with EphA4-positive regions (indicated by cream background at the bottom of Fig. 5). Clusters 2, 5, and 8 belong to this category; clusters 2 and 5 are generated on E11.5 and E12.5, and cluster 8 is generated on E10.5 and E11.5.

To examine the correlation between the cerebellar M-L clusters and patterns of *En-2*, *Wnt-7B,* and *L7/pcp2* expression, we performed whole-mount *in situ* hybridization with antisense RNA probes specific to them (Fig. 6). In E18.5 cerebella, *En-2*, *Wnt-7B,* and *L7/pcp2* are expressed in the specific subsets of the M-L clusters (Fig. 6). The domains of *En-2* expression correspond with clusters 1, 3, and maybe 6 [Fig. 6, *En-2* (E18.5)]. The *En-2*-specific signal in cluster 6 is obscure. The domains of *Wnt-7B* expression correspond with clusters 2, 4/5, and 8 [Fig. 6, *Wnt-7B* (E18.5)]. The expression patterns of *En-2* and *Wnt-7B* complement one other. The domains of *L7/pcp2* expression correspond with clusters 2 and 4 [Fig. 6, *L7/pcp2* (E18.5)]. The positional correlation between the cerebellar M-L clusters and the pattern of *En-2*, *Wnt-7B,* and *L7/pcp2* expression is shown in the diagram at the bottom of Figure 6. These results indicate that PC birth dates closely correlate with the establishment of cerebellar M-L clusters and define the positional identity of each M-L cluster.

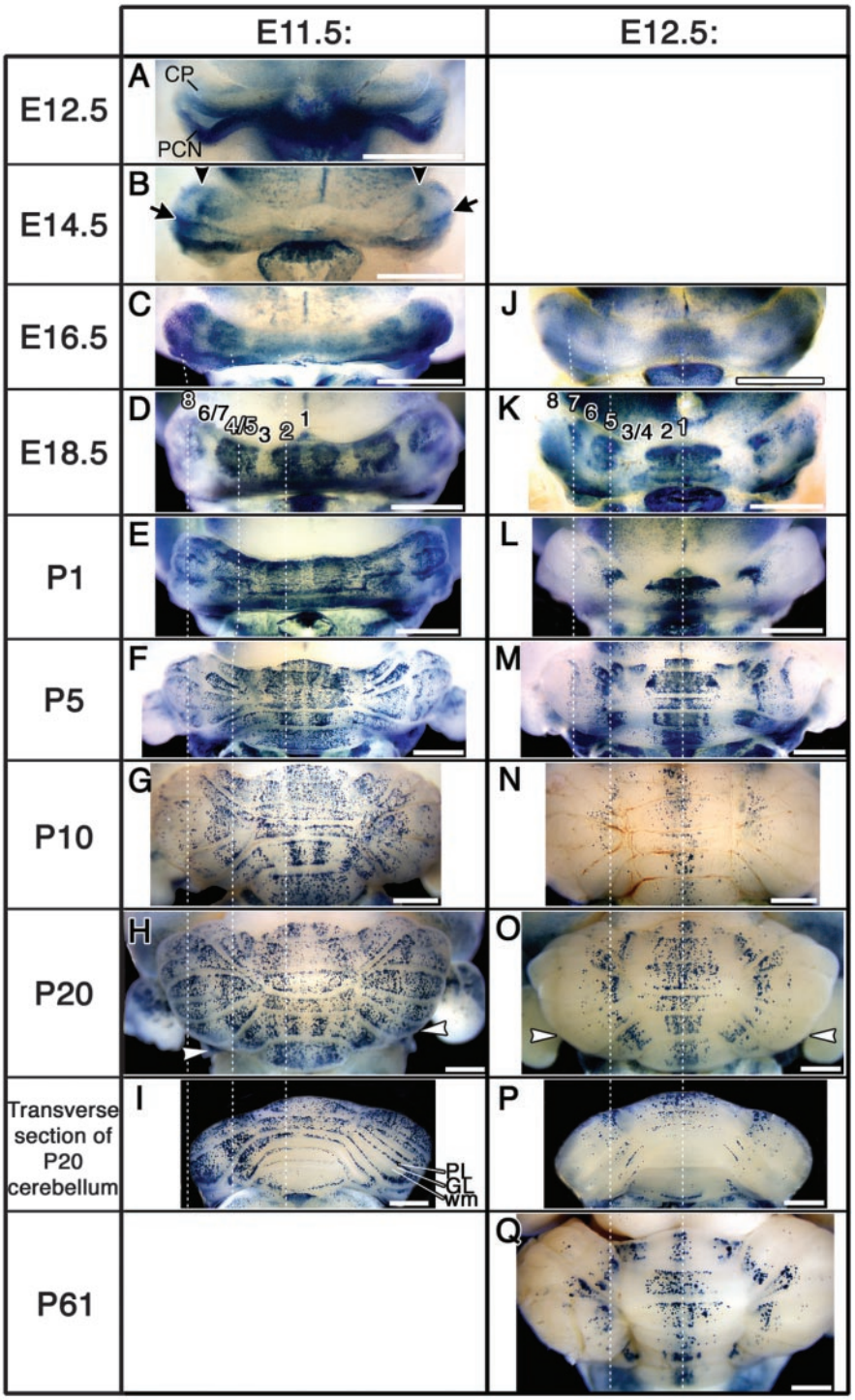

Figure 3. Developmental process forming M-L clusters from E11.5 or E12.5. AdexCAG-NL-LacZ was injected into the midbrain ventricles of embryos at E11.5 (left column) and E12.5 (right column). They were fixed and stained by whole-mount for β-gal (blue) at different developmental stages from E12.5 to P61. All pictures indicate posterior views and were individually magnified so that the cerebellar widths were normalized to the same size. In the left column (E11.5:), the relative positions of clusters 2, 4/5, and 8 are indicated by white dotted lines. The arrows and arrowheads in *B* show independent clusters. In the right column (E12.5:), the relative positions of clusters 1, 5, and 7 are indicated by white dotted lines. The cerebellum in *H* and *O* was sectioned transversely in the region between the arrowheads, as shown in *I* and *P*, respectively. CP, Cerebellar primordium; GL, granular layer; PCN, precerebellar neuroepithelium; wm, white matter. Scale bar, 1 mm.

Ablation of the cerebellar M-L clusters

To examine the function of PC birth date-related M-L clusters, we ablated the M-L clusters of PCs generated on E12.5 (clusters 1, 2, 5, and 7) (Figs. 3, 5) with AdexCAG-HSVtk and GCV (see Materials and Methods).

First, to ascertain whether this treatment can destroy specific M-L clusters, we injected a mixture of AdexCAG-HSVtk and

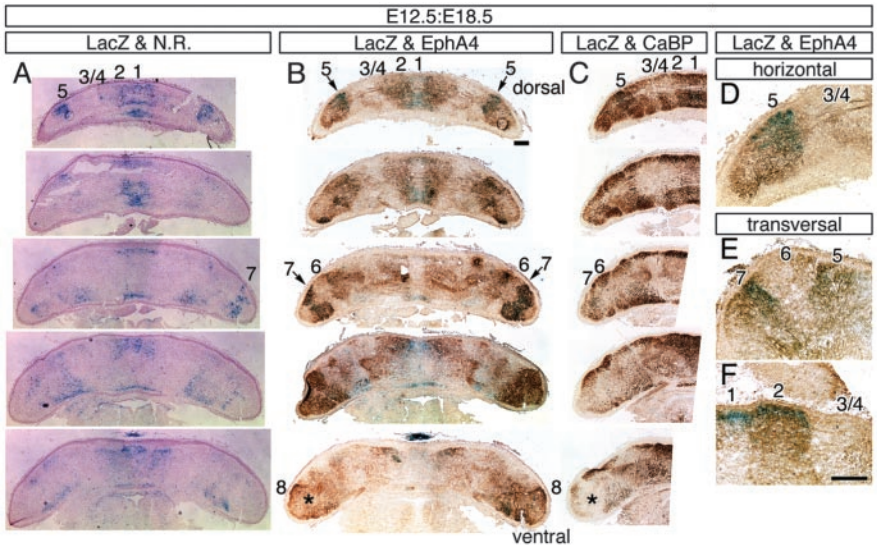

Figure 4. Imunohishochemistry of the E12.5:E18.5 cerebellum. Horizontal sections from the E12.5:E18.5 cerebellum were stained for β-gal and with neutral red (column *A,* LacZ & N.R.), anti-EphA4 (column *B,* LacZ & EphA4), and anti-calbindin D_{28K} (CaBP) (column *C,* LacZ & CaBP). β-gal activity and immunoreactivity are indicated in blue and dark brown, respectively. The asterisk indicates cluster 8. The sections in each line are adjacent. The dorsal area is at the top, and the ventral is at the bottom. A highly magnified view of the top in column *B* is illustrated in *D*. *E* and *F* are transverse sections stained for β-gal and with anti-EphA4. *E* is the adjacent section of Figure 1*A*. Scale bars: *B* (for *A–C*), *F* (for *D–F*), 200 μm.

AdexCAG-NL-LacZ into the midbrain ventricle of E12.5 embryos; subsequently, the pregnant dams were administered with GCV. The GCV-treated embryos were fixed on E18.5 and stained by whole-mount for β-gal (Fig. 7*B*). In comparison with a control that was not treated with GCV (Fig. 7*A*), several β-gal-positive clusters of the GCV-treated embryos disappeared. The cerebellum of GCV-treated embryo (Fig. 7*B*) was sectioned transversely with a cryostat. The neighboring sections were stained with neutral red (supplemental Figure S1, column *A*, available at www.jneurosci.org) and with anti-CaBP antibody (supplemental Figure S1, column *B*, available at www.jneurosci.org), respectively. The sections indicate that β-gal-positive Purkinje cells are clearly eliminated from clusters 1, 2, 7, and medial half of cluster 5 (supplemental Figure S1, column *A*, available at www.jneurosci.org). β-gal-positive regions are observed in the GCV-treated cerebellum (Fig. 7*B*), but β-gal-positive cells exist in random locations deep within the GCV-treated cerebellum and do not form M-L clusters in the same way as in the control (supplemental Figure S1, column *C*, available at www.jneurosci.org). The CaBP-positive cells exist widely in the GCV-treated cerebellum (supplemental Figure S1, column *B*, available at www.jneurosci.org). Remarkably, the CaBP-positive but β-gal negative cells can be observed in the ablated regions (clusters 1, 2, 5, and 7). This indicates that PCs uninfected with the adenoviral vectors replace the disrupted PCs. Granule cells were not directly killed by this manipulation, because no β-gal activity was observed in the GT or EGL (Figs. 2, 4). In addition, inferior olive neurons in the E12.5:E18.5 control brain (Fig. 7*A*) are negative for β-gal (data not shown), indicating that this treatment does not cause degeneration of the climbing fibers. These results indicate that it is possible to disrupt the specific subset of M-L clusters using AdexCAG-HSVtk and GCV.

After injection of AdexCAG-HSVtk on E12.5, the GCV-treated mice were raised and analyzed at P10 (Fig. 7*D,F,H*). Their uninfected littermates, who were not injected with AdexCAG-HSVtk on E12.5, but were treated with GCV, served as controls (Fig. 7*C,E,G*). The controls showed no abnormal behavior or cerebellar morphology. In contrast, the mice injected with AdexCAG-HSVtk and treated with GCV (termed HSVtk+ mice) had abnormal fissure formation (Fig. 7*D*). In particular, the fissure between lobules VIa and VIb disappeared, and the rostrocaudal boundary between the vermis and hemisphere became less well defined (Fig. 7*F*) (the positions of lost fissures are shown by the red lines in Fig. 7*E*).

To analyze in detail the cerebellar abnormalities of the HSVtk+ mouse, we sectioned parasagitally the control and the HSVtk+ cerebella on a cryostat (Fig. 7*G,H*). The parasagittal sections were immunostained with an anti-CaBP antibody (colored by brown) and further counterstained with cresyl violet (colored by blue). In the HSVtk+ cerebellum (Fig. 7*H*), the fissures between lobules I and II, IV and V, and VIa and VIb had completely disappeared (Fig. 7*H*, arrowheads) (the same positions in the control cerebellum are indicated by arrowheads in Fig. 7*G*) and lobules VIII and IX were partially reduced in size. Where the fissures had disappeared (Fig. 7*H*, arrowheads), neither abnormal PC morphology, a gap in CaBP immunoreactivity, nor a reduction in the EGL cell population was observed. In parts of lobules VIII and IX of the HSVtk+ cerebellum (Fig. 7*H*), a loss in number and abnormal morphology of PCs were observed (Fig. 7*H*, inset). The abnormal PCs horizontally expanded their primary dendrites into the space where the lost PCs were normally present, as if to compensate for the lack of PCs. These observations indicate that ablation of a specific subset of M-L clusters causes abnormalities in cerebellar fissure formation.

Discussion

This study used adenoviral vectors to modify genetically the progenitor cells of PCs. This technique allows us to introduce foreign genes into PC progenitor cells in a neuronal birth date-specific manner. The results indicate the following: (1) Cerebellar progenitor cells are fated to form specific M-L clusters after PC birth between E10.5 and E12.5. (2) The pattern of cerebellar M-L clusters closely correlates with the birth date of their constituent PCs. (3) In contrast to the expression of available M-L markers, the eight M-L clusters themselves are unchanged from embryonic stages to adulthood. (4) There is a correlation between the M-L clusters and the domains of *En-2*, *Wnt-7B*, *L7/pcp2*, and EphA4 expression.

Molecular mechanisms of M-L cluster formation

Each pattern of M-L clusters at late embryonic stages (Figs. 4–6) has been compared with other published observations (Oberdick et al., 1993; Millen et al., 1995). The domains of *En-2* expression at E18.5 correspond to clusters 1 and 3. In addition, cluster 6 may express *En-2* genes. *En-2* may be a candidate for a regulatory factor of a variety of molecules expressed within clusters 1, 3, and 6. For instance, the misexpression of *En-2* induces both ephrin-A2 and ephrin-A5 expression in chick optic tectum (Shigetani et al., 1997). In addition, *En* genes play an important

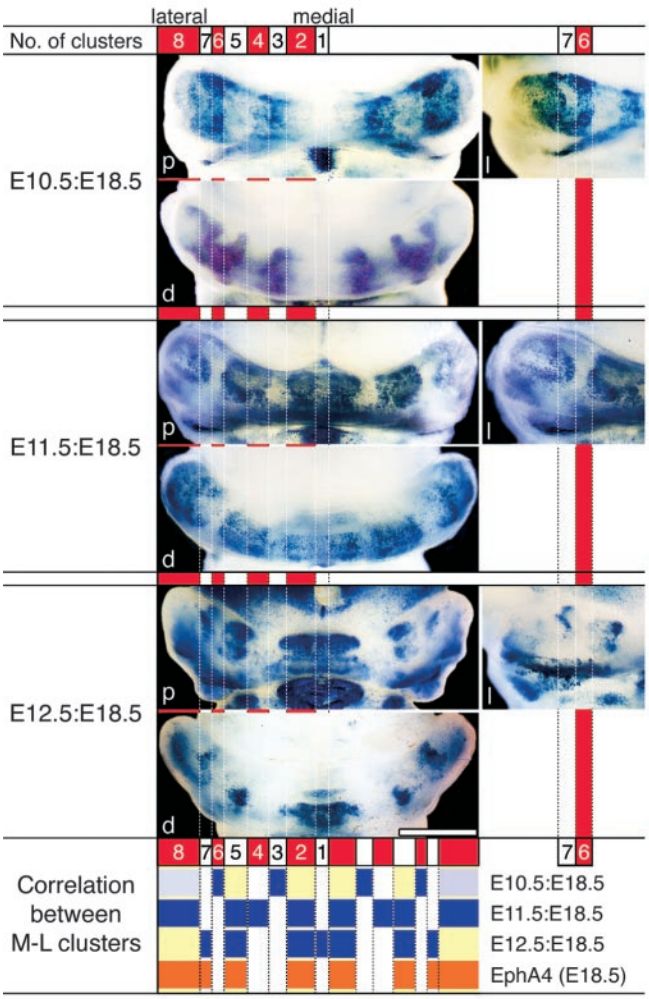

Figure 5. Comparison of M-L cluster patterns at E18.5. The posterior (*p*), dorsal (*d*), and near lateral (*l*) views of E10.5:E18.5, E11.5:E18.5, and E12.5:E18.5 cerebella are indicated in each line. The positions of M-L clusters are defined and named from 1 to 8. The M-L cluster number is shown at the top of the lines. The boundaries of M-L clusters are indicated by dotted lines. The spatial relationship of the M-L clusters in E10.5:E18.5, E11.5:E18.5, E12.5:E18.5 cerebella and EphA4-positive regions in the E18.5 cerebellum (refer to Fig. 4) is shown in a diagram at the bottom of the lines. Scale bar, 1 mm.

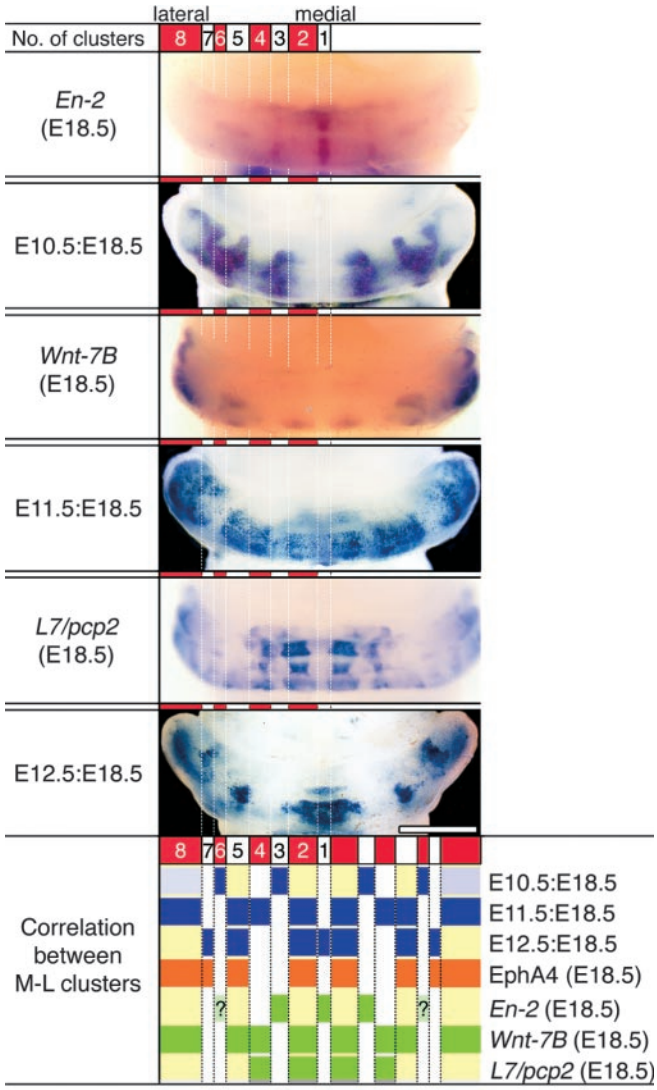

Figure 6. Comparison with patterns of *En-2*, *Wnt-7B,* and *L7/pcp2* expression. E18.5 cerebella were whole-mount hybridized with antisense RNA probes specific to *En-2*, *Wnt-7B,* and *L7/pcp2* genes. The patterns of *En-2*, *Wnt-7B,* and *L7/pcp2* expression in E18.5 cerebella are compared with the PC birth date-related M-L clusters. Their positional correlation is shown in the diagram at the bottom. All pictures indicate dorsal views of them. Scale bar, 1 mm.

role in the control of axon guidance (Logan et al., 1996; Shigetani et al., 1997). One consequence may be that EphA4-expressing climbing fibers cannot enter clusters 1, 3, and 6 because ephrin-A5 repels EphA4-positive axons (Walkenhorst et al., 2000). Hence, clusters 1, 3, and 6 are completely negative for EphA4 immunoreactivity (Fig. 4). Moreover, this model may explain why β-gal-positive PCs in clusters 2, 5, and 7 do not invade adjacent clusters 3 and 6 in the E12.5:E18.5 cerebellum (Fig. 4*D–F*). The EphA4-positive regions may provide a migration path for PCs in clusters 2, 5, and 7, or clusters 3 and 6 may be repulsive to PCs in cluster 2, 5, and 7. It is unclear, however, whether the M-L PC clusters or regional expression of EphA4 is established first.

The locations of clusters 2, 4/5, and 8, which are complementary to 1, 3, and 6, correspond to the pattern of *Wnt-7B* expression (Fig. 6). *Wnt-7B* may be involved with the regulation of a variety of molecules expressed within clusters 2, 4/5, and 8, but the potential role of *Wnt-7B* in M-L cluster formation is unknown. The identity of each M-L cluster may be maintained by a special cell surface adhesion molecule or signal molecules mediating cell–cell interaction, so that PCs in neighboring M-L clusters do not mingle with each other.

Interestingly, the *En-2*-positive clusters 3 and 6, but not cluster 1, are generated from the ventricular zone on E10.5 (Figs. 5, 6), whereas the *Wnt-7B*-positive clusters 2, 4/5, and 8 are generated on E11.5 (Figs. 5, 6). It appears that there is a correlation between PC birth date and *En-2* and *Wnt-7B* expression patterns.

Developmental processes in M-L cluster formation

The cell lineage of PCs has been examined using an adenovirus-mediated gene transfer system (M. Hashimoto and K. Mikoshiba, unpublished observations). The results indicated that PC progenitor cells on the ventricular surface of the fourth ventricle generated clonally related PCs spanning many M-L clusters (data not shown). This result is consistent with earlier studies suggesting that clonally related PCs do not define the M-L cluster-like

distribution in the cerebellar cortex (Baader et al., 1996; Hawkes et al., 1998). Thus, the PC progenitor cells are multipotent, and the ventricular zone of the fourth ventricle may not be composed of distinct subpopulations of progenitor cells fated to form the specific M-L clusters.

The results indicate that newly born PCs are committed to form specific M-L clusters at birth. This behavior is analogous to the determination of laminar identity in cortical neurogenesis (McConnell and Kaznowski, 1991). However, the establishment of cerebellar structure is more complex than cortical laminar formation because the M-L clusters are formed in a nested manner. Moreover, each cortical layer is distinguishable in its morphology and functional properties (for review, see McConnell, 1988), distinctions that cannot be made in M-L clusters due to the homogeneity of the PCs that comprise them.

One day after injection (E11.5:E12.5), β-gal-positive cells in the cerebellum occupied the ventricular zone and did not form a distinct subpopulation (Fig. 8*A*). Only later did they form two independent subgroups (Figs. 3*B,* 8*B,* arrows and arrowheads) within the developing cortex [mantle zone (MZ)] of E11.5:E14.5 cerebellum (data not shown). Furthermore, the subgroup forming the laminar structure (Figs. 3*B,* 8*B,* arrows) appears to be restricted to a specific region within the E11.5:E16.5 cerebellum to form an M-L cluster (Fig. 8*C,D*, arrow). These results indicate that for a few days after PCs are generated from the ventricular surface, they do not form subpopulations in the ventricular zone, but they do eventually divide into subgroups within the MZ.

Therefore, we hypothesize that the pattern of cerebellar M-L clusters is generated through two independent steps. The first is a "generation step" in VZ, and the second is a "subdividing step" in the MZ. In the generation step, the first PCs to be generated, on E10.5, immediately acquire their cell fate, characterized by the expression of *En-2* and *En-2*-regulated molecules. One the next day (E11.5), newly generated E11.5 PCs are exposed to some extrinsic signals from the E10.5 PCs. These signals affect the cell fate of the newly generated E11.5 PCs such that they acquire a different cell identity from the E10.5 PCs and are characterized by the expression of *Wnt-7B* and *Wnt-7B*-regulated molecules. In the subdividing step, each subset of PCs leaves the VZ and migrates into the MZ without mingling with each other. They are exposed to extrinsic cues such as EphA4 that play a role in subdividing them into distinct M-L clusters. The PCs choose migration paths or regions according to their identities and the extrinsic signals. Consequently, PCs are subdivided into subgroups, and the nested M-L clusters are formed.

The relationship between M-L clusters and foliation

In HSVtk+ mice at P10 (Fig. 7*D*), the greatest loss of fissures is observed at the midline of the vermis and in the paravermian region. This abnormal foliation is caused by the loss of PCs that comprise clusters 1, 2, 5, and 7. However, anti-CaBP immunohistochemistry indicates that there is no PC gap and that the morphology of PCs is normal in the locations within the midline of vermis where fissures are missing (Fig. 7*H,* clusters 1 and 2, arrowheads) because the disrupted PCs are replaced by PCs from neighboring M-L clusters during cerebellar development (supplemental Figure S1, available at www.jneurosci.org). If each M-L cluster presents positional information to its surroundings, the replacement cell may not be able to compensate

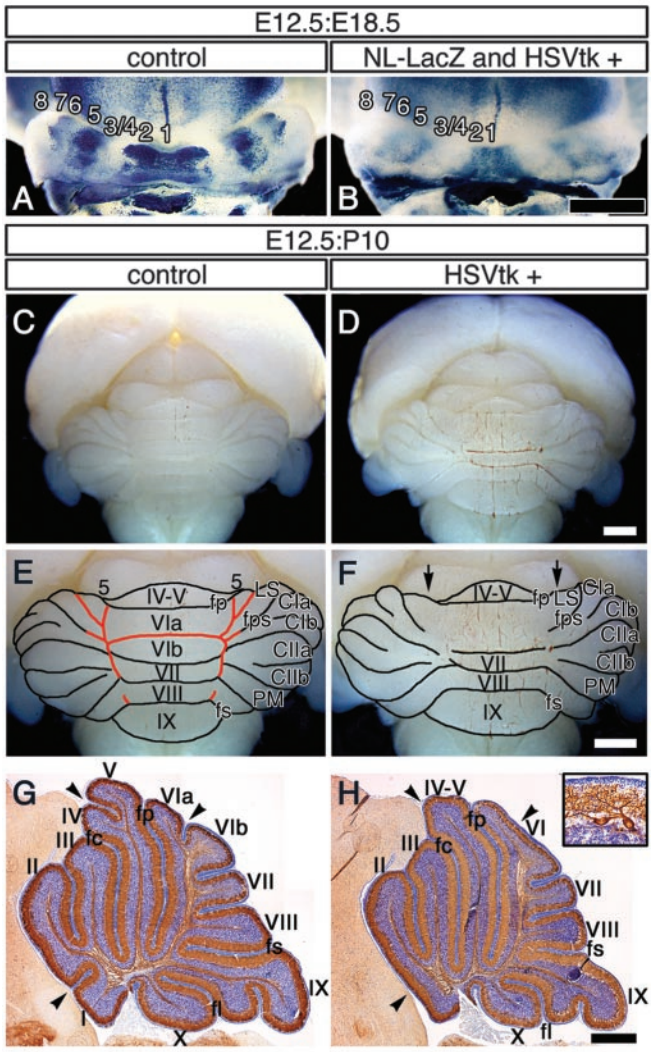

Figure 7. Ablation of the M-L clusters with AdexCAG-HSVtk and GCV. To examine the function of M-L clusters, M-L clusters 1, 2, 5, and 7 were destroyed by AdexCAG-HSVtk and GCV. A mixture of AdexCAG-NL-LacZ and AdexCAG-HSVtk was injected into the midbrain ventricle of mouse embryo on E12.5. *A* and *B* show posterior views of E12.5:E18.5 cerebella stained by whole-mount for β-gal. *B* and *A* show GCV-treated and -untreated cerebella, respectively. *C–H* show E12.5:P10 cerebella. An E12.5:P10 cerebellum in which the M-L clusters were destroyed by AdexCAG-HSVtk and GCV (HSVtk+) is indicated in *D*, *F*, and *H*. A cerebellum from a littermate that was not injected with AdexCAG-HSVtk is shown in *C*, *E*, and *G* as a control. The cerebellar fissures of *C* and *D* are illustrated in *E* and *F*, respectively. The arrows in *F* indicate the positions of cluster 5 in the normal E12.5:P10 cerebellum (5 in *E* refers to Fig. 3*N*). Red lines in *E* indicate the positions where fissures are missing in *F*. Parasagittal sections were cut from *E* and *F* and stained with anti-CaBP (brown) and cresyl violet (blue) (*G, H*). A parasagittal section of the E12.5:P10 cerebellum of an HSVtk+ mouse (*H*) indicates abnormal fissure formation. The arrowheads in *G* and *H* indicate the positions of the missing fissures. The inset in *H* shows an abnormal PC in lobule IX. I-X, Lobules I-X; fc, preculminate fissure; fl, posterolateral fissure. Scale bars: *B* (for *A, B*), *D* (for *C, D*), *F* (for *E, F*), 1 mm; *H* (for *G, H*), 0.5 mm; *H*, inset, 0.2 mm.

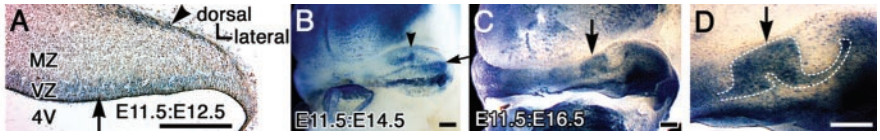

Figure 8. Process of M-L cluster formation. A transverse section of E11.5:E12.5 cerebellum (Fig. 3*A*) stained for β-gal and anti-ephrin A2 is shown in *A*. The β-gal-positive cells (blue) do not form subpopulations in the VZ (arrow: presumptive PC). Presumptive deep nuclear neurons in the dorsal region are indicated by arrowheads. Lateral views of E11.5:E14.5 (Fig. 3*B*) and E11.5:E16.5 (Fig. 3*C*) cerebella are shown in *B* and *C*, respectively. A magnified view of an M-L cluster (arrow in *C*) is indicated in *D*, and its shape is traced by the white dotted line. 4V, Fourth ventricle; MZ, marginal zone; VZ, ventricular zone. Scale bar, 0.25 mm.

sufficiently for the disruption because it does not have accurate positional information. It is unclear what the positional information is. Abnormal foliation may also result from a reduction in cell population within the EGL, given the previous proposal that cerebellar fissures are generated by the buckling forces produced by the more rapid expansion of EGL relative to the cerebellar cortex (Mares and Lodin, 1970; Lauder et al., 1974). Sonic hedgehog protein derived from PCs promotes the proliferation of granule neuron precursors in EGL, suggesting that the size of the EGL population is determined by the number of PCs (Wechsler-Reya and Scott, 1999). Thus, a reduction in PC population decreases the size of the EGL cell population and, furthermore, diminishes foliation. Many studies of autistic patients have identified reductions of PC numbers and hypoplasia in cerebellar vermal lobules (for review, see Courchesne, 1997), but it is unclear whether PC loss underlies the autistic behavior or not. Interestingly, the abnormal fissure formations of HSVtk+ mouse are restricted to the vermal and paravermal regions (Fig. 7). If this HSVtk+ mouse is examined in detail, we will obtain new information on a correlation between PC loss and associated behavior deficits.

In conclusion, these observations indicate that the birth date of PCs determines the formation of M-L clusters and fissures in the mouse cerebellum. However, the molecular mechanisms by which M-L clusters are formed are still obscure. Using our technique of adenoviral infection, it is possible to modify genetically each individual M-L cluster, aiding in the study of these developmental mechanisms.

References

Altman J, Bayer SA (1978) Prenatal development of the cerebellar system in the rat. I. Cytogenesis and histogenesis of the deep nuclei and the cortex of the cerebellum. J Comp Neurol 179:23–48.

Baader SL, Schilling ML, Rosengarten B, Pretsch W, Teutsch HF, Oberdick J, Schilling K (1996) Purkinje cell lineage and the topographic organization of the cerebellar cortex: a view from X inactivation mosaics. Dev Biol 174:393–406.

Bloedel JR, Kelly TM (1991) The dynamic selection hypothesis: a proposed function for cerebellar sagittal zones. In: The cerebellum revisited (Llinás R, Sotelo C, eds), pp 267–282. New York: Springer.

Chen G, Hanson CL, Ebner TJ (1996) Functional parasagittal compartments in the rat cerebellar cortex: an in vivo optical imaging study using neutral red. J Neurophysiol 76:4169–4174.

Chockkan V, Hawkes R (1994) Functional and antigenic maps in the rat cerebellum: zebrin compartmentation and vibrissal receptive fields in lobule IXa. J Comp Neurol 345:33–45.

Courchesne E (1997) Brainstem, cerebellar and limbic neuroanatomical abnormalities in autism. Curr Opin Neurobiol 7:269–278.

Garwicz M (2000) Micro-organisation of cerebellar modules controlling forelimb movements. Prog Brain Res 124:187–199.

Gravel C, Hawkes R (1990) Parasagittal organization of the rat cerebellar cortex: direct comparison of Purkinje cell compartments and the organization of the spinocerebellar projection. J Comp Neurol 291:79–102.

Gravel C, Eisenman LM, Sasseville R, Hawkes R (1987) Parasagittal organization of the rat cerebellar cortex: direct correlation between antigenic Purkinje cell bands revealed by mabQ113 and the organization of the olivocerebellar projection. J Comp Neurol 265:294–310.

Hallem JS, Thompson JH, Gundappa-Sulur G, Hawkes R, Bjaalie JG, Bower JM (1999) Spatial correspondence between tactile projection patterns and the distribution of the antigenic Purkinje cell markers anti-zebrin I and anti-zebrin II in the cerebellar folium crus IIA of the rat. Neuroscience 93:1083–1094.

Hashimoto M, Aruga J, Hosoya Y, Kanegae Y, Saito I, Mikoshiba K (1996) A neural cell-type-specific expression system using recombinant adenovirus vectors. Hum Gene Ther 7:149–158.

Hawkes R (1997) An anatomical model of cerebellar modules. Prog Brain Res 114:39–52.

Hawkes R, Gravel C (1991) The modular cerebellum. Prog Neurobiol 36:309–327.

Hawkes R, Faulkner-Jones B, Tam P, Tan SS (1998) Pattern formation in the cerebellum of murine embryonic stem cell chimeras. Eur J Neurosci 10:790–793.

Herrup K, Kuemerle B (1997) The compartmentalization of the cerebellum. Annu Rev Neurosci 20:61–90.

Ito M (1984) The cerebellum and neural control. New York: Raven.

Karam SD, Burrows RC, Logan C, Koblar S, Pasquale EB, Bothwell M (2000) Eph receptors and ephrins in the developing chick cerebellum: relationship to sagittal patterning and granule cell migration. J Neurosci 20:6488–6500.

Lauder JM, Altman J, Krebs H (1974) Some mechanisms of cerebellar foliation: effects of early hypo- and hyperthyroidism. Brain Res 76:33–40.

Leclerc N, Gravel C, Hawkes R (1988) Development of parasagittal zonation in the rat cerebellar cortex: MabQ113 antigenic bands are created postnatally by the suppression of antigen expression in a subset of Purkinje cells. J Comp Neurol 273:399–420.

Lobe CG, Koop KE, Kreppner W, Lomeli H, Gertsenstein M, Nagy A (1999) Z/AP, a double reporter for cre-mediated recombination. Dev Biol 208:281–292.

Logan C, Wizenmann A, Drescher U, Monschau B, Bonhoeffer F, Lumsden A (1996) Rostral optic tectum acquires caudal characteristics following ectopic engrailed expression. Curr Biol 6:1006–1014.

Mares V, Lodin Z (1970) The cellular kinetics of the developing mouse cerebellum. II. The function of the external granular layer in the process of gyrification. Brain Res 23:343–352.

Mathis L, Bonnerot C, Puelles L, Nicolas JF (1997) Retrospective clonal analysis of the cerebellum using genetic laacZ/lacZ mouse mosaics. Development 124:4089–4104.

McConnell SK (1988) Development and decision-making in the mammalian. Brain Res Rev 13:1–23.

McConnell SK, Kaznowski CE (1991) Cell cycle dependence of laminar determination in developing neocortex. Science 254:282–285.

Millen KJ, Hui CC, Joyner AL (1995) A role for En-2 and other murine homologues of *Drosophila* segment polarity genes in regulating positional information in the developing cerebellum. Development 121:3935–3945.

Miyake S, Makimura M, Kanegae Y, Harada S, Sato Y, Takamori K, Tokuda C, Saito I (1996) Efficient generation of recombinant adenoviruses using adenovirus DNA- terminal protein complex and a cosmid bearing the full-length virus genome. Proc Natl Acad Sci USA 93:1320–1324.

Muneoka K, Wanek N, Bryant SV (1986) Mouse embryos develop normally exo utero. J Exp Zool 239:289–293.

Niwa H, Yamamura K, Miyazaki J (1991) Efficient selection for high-expression transfectants with a novel eukaryotic vector. Gene 108:193–199.

Oberdick J, Schilling K, Smeyne RJ, Corbin JG, Bocchiaro C, Morgan JI (1993) Control of segment-like patterns of gene expression in the mouse cerebellum. Neuron 10:1007–1018.

Oberdick J, Baader SL, Schilling K (1998) From zebra stripes to postal zones: deciphering patterns of gene expression in the cerebellum. Trends Neurosci 21:383–390.

Oscarsson O (1980) Functional organization of olivary projection to cerebellar anterior lobe. In: The inferior olivary nucleus (Courville J, de Montigny C, Lamarre Y, eds), pp 279–289. New York: Raven.

Osumi-Yamashita N, Kuratani S, Ninomiya Y, Aoki K, Iseki S, Chareonvit S, Doi H, Fujiwara M, Watanabe T, Eto K (1997) Cranial anomaly of homozygous rSey rat is associated with a defect in the migration pathway of midbrain crest cells. Dev Growth Differ 39:53–67.

Paradies MA, Grishkat H, Smeyne RJ, Oberdick J, Morgan JI, Eisenman LM (1996) Correspondence between L7-lacZ-expressing Purkinje cells and labeled olivocerebellar fibers during late embryogenesis in the mouse. J Comp Neurol 374:451–466.

Robertson LT, Laxer KD (1981) Localization of cutaneously elicited climbing fiber responses in lobule V of the monkey cerebellum. Brain Behav Evol 18:157–168.

Shigetani Y, Funahashi JI, Nakamura H (1997) En-2 regulates the expression of the ligands for Eph type tyrosine kinases in chick embryonic tectum. Neurosci Res 27:211–217.

Turner DL, Cepko CL (1987) A common progenitor for neurons and glia persists in rat retina late in development. Nature 328:131–136.

Voogd J, Bigare F (1980) Topographical distribution of olivary and corticonuclear fibers in the cerebellum: a review. In: The inferior olivary nucleus (Courville J, de Montigny C, Lamarre Y, eds), pp 207–234. New York: Raven.

Voogd J, Glickstein M (1998) The anatomy of the cerebellum. Trends Neurosci 21:370–375.

Walkenhorst J, Dutting D, Handwerker C, Huai J, Tanaka H, Drescher U (2000) The EphA4 receptor tyrosine kinase is necessary for the guidance of nasal retinal ganglion cell axons in vitro. Mol Cell Neurosci 16:365–375.

Wassef M, Angaut P, Arsenio-Nunes L, Bourrat F, Sotelo C (1991) Purkinje cell heterogeneity: its role in organizing the topography of the cerebellar cortex connections. In: The cerebellum revisited (Llinás R, Sotelo C, eds), pp 5–21. New York: Springer.

Wechsler-Reya RJ, Scott MP (1999) Control of neuronal precursor proliferation in the cerebellum by Sonic Hedgehog. Neuron 22:103–114.

Wigler M, Pellicer A, Silverstein S, Axel R (1978) Biochemical transfer of single-copy eucaryotic genes using total cellular DNA as donor. Cell 14:725–731.

Wilkinson DG (2001) Multiple roles of EPH receptors and ephrins in neural development. Nat Rev Neurosci 2:155–164.

Zhao H, Ivic L, Otaki JM, Hashimoto M, Mikoshiba K, Firestein S (1998) Functional expression of a mammalian odorant receptor. Science 279: 237–242.